

AN UNCERTAINTY PROPAGATION IN DEVELOPED VISION BASED MEASUREMENT SYSTEM AIDED BY NUMERICAL AND EXPERIMENTAL TESTS

PIOTR KOHUT, KRZYSZTOF HOLAK, ADAM MARTOWICZ

AGH University of Science and Technology, Department of Robotics and Mechatronics, Kraków, Poland

e-mail: pko@agh.edu.pl; holak@agh.edu.pl; adam.martowicz@agh.edu.pl

In the paper, the vision-based method of static in-plane deflection measurement of a structure is presented. Displacements of measurement points of the structure under the load are computed by means of the normalized digital image correlation coefficient. The application of the homography transformation enables the deflection field to be computed from two images of the structure acquired from distinct points in space. The scale coefficient calculation and marker matching algorithms have been introduced in order to increase the level of automation of the method. The paper presents the results of numerical investigations of the uncertainty propagation in the proposed algorithms. The qualitative comparison of the numerical data and the results of the experiment have been shown.

Key words: digital image correlation, homography mapping, vision system

1. Introduction

The vision systems for measurement of motion and three-dimensional geometry of objects have become more available on the market. However, their number is still small in the field of measurement of deformations, damage detection and localization. In diagnostics of civil engineering structures, measurements of displacements are the major aspect of evaluation of static states and dynamic characteristics of constructions (Uhl, 2009). The application of traditional transducers like accelerometers or strain gauge sensors requires their direct contact with examined elements of structures while carrying out an experiment. In many cases, it is very difficult or even impossible in practical working conditions of such devices. There is a need to design and implement of other, non-contact measurement systems. In such cases, the vision systems, as easy to use, accurate and universal tool can be a good alternative for deflections and deformations measurements (Uhl *et al.*, 2009a,b; Giergiel and Kohut, 2008). Displacement measurements allow damage detection to be performed by means of change in the structure global geometry, such as deflection curve, analysis.

The measurement system can be characterized by its accuracy and uncertainty. These features become important in the design of structural health monitoring systems, which have to make a correct decision about the state of the objects automatically or predict their lifetime and probability of future failure. The nature of real measurements involves uncertainty (Borner *et al.*, 2009; Santo *et al.*, 2004). Limited quality of measurement equipment results in the variation of yielded outcomes. Therefore, the use of both the sensitivity analysis and the assessment of uncertainty propagation seems to be justified (Moens and Vandepitte, 2006). They can be carried out to confirm the quality of optical tools applied in the area of SHM (Giurgiutiu, 2008).

A deterministic evaluation of measurement methods introduces no information about how the measured response varies in presence of identified uncertainties. The solution that helps to overcome the mentioned inconvenience could be a series of measurements performed in order to determine required statistics. Stochastic analyses allow one to look for the relationships between input and output parameters as well as to find the best configuration of measurement equipment which characterizes the least sensitivity to the present uncertainty. Identified uncertainties can be modeled e.g. as random numbers or fields, intervals and fuzzy numbers (Moens and Vandepitte, 2005). In the case of random numbers, they are represented with statistics of chosen orders, e.g. mean, standard deviation or probability density functions (PDF). Random fields stand for an extension of random numbers since they are used with spatial PDF with an assumed correlation between input characteristics e.g. defined with the correlation length (Schueller, 1997).

There are distinguished probabilistic and possibilistic computational techniques for the assessment of the uncertainty propagation. The first group can deal with random numbers and fields. The Monte Carlo simulation (MCS) is commonly applied to find PDF and required statistics (Schueller, 1997). The latter group can be used in the case of intervals and fuzzy numbers (Moens and Vandepitte, 2005; Dubois and Prade, 1980). The most known computational methods are: interval analysis, vertex method, fuzzy sets theory including the Zadeh extension principle and the transformation method with its several improvements (Hanss, 2005). As an alternative to the fuzzy numbers, application of the effective alpha-cut strategy can be also considered (Donders *et al.*, 2005). Uncertainty analyses make the results of numerical simulations to be closer to real experiments. They also help to understand the true nature of phenomena present in mechanical structures.

In this paper, the developed vision based method dedicated for in-plane measurement of displacement fields of civil engineering structures is presented. The deflection curve is obtained from two images of the construction: the referential one and the one acquired after application of the load. The paper presents the results of numerical investigations of the uncertainty propagation in the homography computation as well as deflection measurement algorithms. The results of the simulation in MATLAB environment are compared with the experimental data.

2. The vision in-plane deflection measurement method

The developed vision based method for the in-plane deflection measurement consists of three basic steps (Uhl *et al.*, 2009a): the calibration of the camera, rectification and the measurement of the in-plane displacement of the structure. In the first step, the scale coefficient is calculated from images of markers with known geometric dimensions. Next, the reference image and one or more images of the construction under the load are acquired. The next step of the algorithm is necessary if successive photographs are taken from distinct points in space. The matrix \mathbf{H} is calculated from the set of markers coplanar with the plane of the construction. The mapping \mathbf{H} transforms the images and removes the projective distortions from the image of one plane of the structure. After the transformation, the photographs acquired from different points in space can be overlaid with the reference image. In the last step, the image of the construction plane is divided into a dense grid of intensity patterns. The deflection curve is computed with the help of the normalized cross correlation coefficient (NCC). The sub-pixel techniques are introduced to increase the accuracy of the measurement. The beam deflection is rescaled to metric units using the known scale coefficient.

2.1. Calibration of the system

The scale coefficient $\alpha_{mm/pix}$ is computed from the object with known geometric dimensions. It can be obtained from planar circular or rectangular markers or from a certified length standard.

Two different methods of the scale calibration were implemented in the system. The first one makes use of the binary image of the calibration pattern, the second one introduces Hough's transform for circle detection and ellipse fitting technique. The full calibration is carried out to obtain the intrinsic calibration matrix \mathbf{K} . The chessboard planar pattern with black and white squares, an even number of rows and odd number of columns is used. The set of 4 radial and tangential lens distortion coefficients are also calculated by means of the internal calibration (Uhl *et al.*, 2009b).

2.2. Planar homography transformation

The homography (Hartley and Zisserman, 2004; Ma *et al.*, 2004) is a mapping between two sets of points on the plane. If coplanar point positions are given in homogenous coordinates, the homography can be represented by a 3-by-3 matrix denoted as \mathbf{H} . In general, the matrix \mathbf{H} represents the full projective transformation and consists of similarity (translation, rotation and scaling), affine and projective transformations (Fig. 1). The transformation which maps coplanar points on the image with projective distortions to corresponding points on the reference image is given by

$$\mathbf{x} = \mathbf{H}\mathbf{x}' \tag{2.1}$$

where \mathbf{H} is the homography transformation matrix.

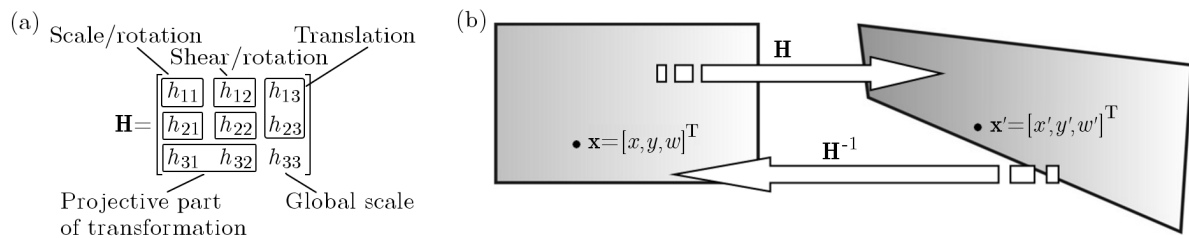


Fig. 1. (a) Homography matrix elements, (b) action of homography mapping on the plane

In Fig. 1, the matrix elements h_{13} and h_{23} represent translation, elements of the upper left 2×2 sub-matrix are associated with rotation, shear transformation and scaling. The third row of the matrix \mathbf{H} carries information about the perspective and non uniform foreshortenings. The last element h_{33} of the normalized homography matrix is equal to 1. The matrix \mathbf{H} is computed from a set of corresponding points by the DLT algorithm. At least four pairs of coplanar corresponding points are necessary and sufficient for computation of the matrix \mathbf{H} if none three of them are collinear and the system of equation (2.1) is solved by the least squares method (DLT). The results of the rectification performed on the lab setup image are presented in Fig. 2.



Fig. 2. (a) Reference image of the unloaded structure, (b) image of the loaded frame captured with projective distortions; (c) image rectified by the homography matrix computed from coplanar rectangular markers

2.3. Correlation coefficient

The value of the normalized cross correlation coefficient (NCC) in the pixel of the image region is equal to the degree of similarity between the region centered on that pixel and a given intensity template (Orteu, 2009; Ma *et al.*, 2004). The normalized cross correlation coefficient value equal to 1 corresponds to a region on the image that is exactly the same as the intensity pattern. It is given by equation (2.2)

$$NCC(u, v) = \frac{\sum_{x,y} [f_n(x, y) - \bar{f}_n][f_d(x - u, y - v) - \bar{f}_d]}{\sqrt{\sum_{x,y} [f_n(x, y) - \bar{f}_n]^2 \sum_{x,y} [f_d(x - u, y - v) - \bar{f}_d]^2}} \quad (2.2)$$

where: $f_n(x, y)$ is the intensity value for the image patch (x, y) on the reference image, \bar{f}_n – mean value of the image patch on the reference image, $f_d(x - u, y - v)$ – intensity value for the image patch on the image after deformation, \bar{f}_d – mean value of the image patch on the analyzed image, u, v – displacement of the pattern between two images.

In the measurement process, the reference image of the unloaded structure is divided into intensity patterns (Fig. 3a). The position of each of the intensity patterns is calculated on both images: the referential one and the one after the applied rectification. The displacement vector for each measurement point is computed as a difference between positions of the pattern on two images. The method applied to each point of interest gives a complete course of deflection of the analyzed object (Fig. 3b). The correlation coefficient computes the discrete position of the pixel on the image. When the sub-pixel methods are introduced, one can increase the measurement accuracy up to 0.01-0.1 parts of the pixel.

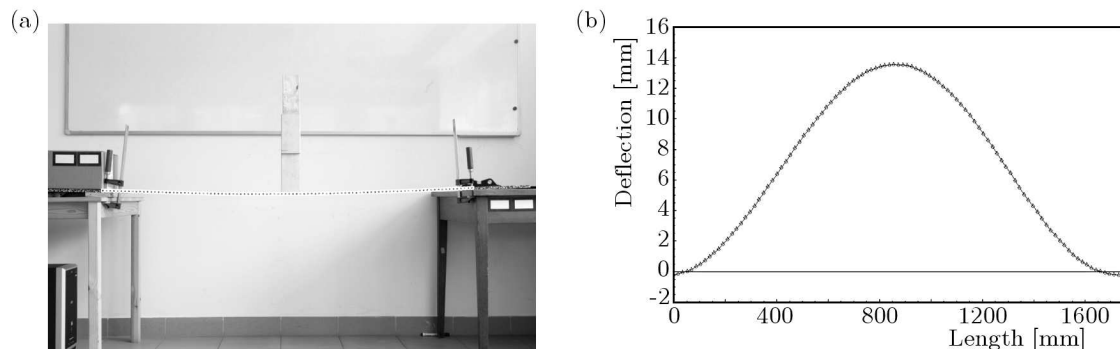


Fig. 3. (a) Beam divided into intensity patterns – dense division, (b) deflection curve obtained by the optical measurement method

3. Numerical tests

The main goal of the numerical simulation of the developed method was the uncertainty analysis of the homography matrix elements and deflection curve. The model of the scene was implemented in MATLAB software. It consisted of the pin hole camera model (Ma *et al.*, 2004) and the virtual structure. The acquisition of the image by a camera was modeled as a central projection with the center in the origin of the camera coordinate system. The camera had known set of internal $(f, s_x, s_y, u_0, v_0, s_\theta = 0)$ and external parameters (\mathbf{R}, \mathbf{T}) . The virtual camera with 21.1 Mega pixel resolution and lens with 4 different focal lengths ($f = 12 \text{ mm}, 35 \text{ mm}, 50 \text{ mm}$ and 80 mm) was modeled. Each focal length was associated with the reference distance between the camera and the structure, which have been summarized in Table 1. The model of the structure consisted of a simply supported beam loaded by a point force acting centrally and a set of markers coplanar with the beam plane necessary for rectification. The FEM model of

the beam was constructed in MATLAB from 1D Euler beam elements. The steel beam of length 800 mm, cross section area 500 mm^2 and Young's modulus equal to $2.1 \cdot 10^5 \text{ MPa}$ was modeled. The structure was loaded by a point force of magnitude 1000 N. The set consisting of 6 markers was positioned symmetrically with respect to the structure (Fig. 4). The following cases were investigated in the analysis of variability of the homography matrix elements and the measured deflection of the beam: 1) change of the camera orientation with respect to the normal plane of the structure and 2) standard deviation of the noise imposed on the coordinates of the markers used for homography estimation.

Table 1. Focal lengths used in simulations with the associated reference distance to the structure

Focal length f [mm]	12	35	50	80
Reference distance d_0 [mm]	500	1200	1500	2500

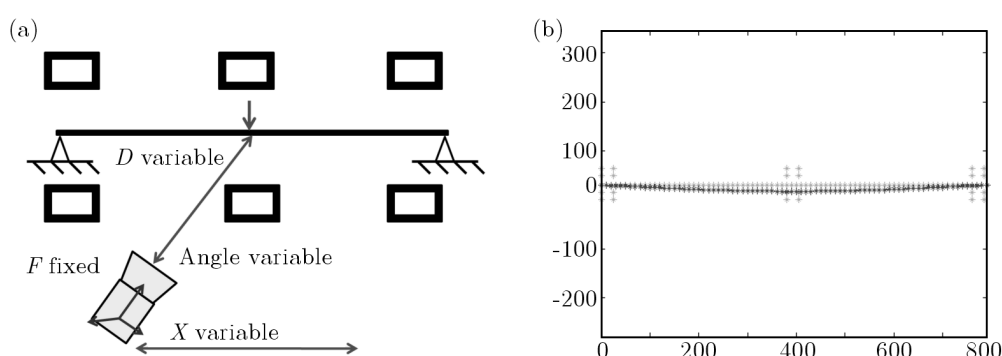


Fig. 4. (a) Camera setup modeled in the simulations: pin hole camera with variable orientation with respect to the structure, (b) acquired virtual image of the beam

The uncertainty is considered for all the corner coordinates of 6 markers used in the simulations. A random noise described by the normal probability distribution function is added to the nominal values of both vertical and horizontal coordinates of corner points. For each investigated case, three standard deviations attached to the localizations of marker corners, i.e.: 0.05, 0.5, 1.0 defined with pixels as units are assumed.

In the next discussion, the following notation concerning the simulation experiment, will be used: each measurement series will be designated as $fXdY$, where X is the focal length [mm], Y – reference distance for a given focal length [mm], for example: $f50d1800$ means the images obtained by a virtual camera with focal length 50 mm and the reference distance $d = 1800$ mm.

3.1. Tests results

The simulation deals with the uncertainty propagation in the case with the camera orbiting around the object. The camera was moved along a circular path around the beam and at the same time, the angle between the optical axis of the camera and the direction perpendicular to the beam plane was varied so that the optical axis always pointed at the center of the beam. The internal parameters were fixed during the investigation (Fig. 4). The assumed standard deviations of computed localizations of marker corners were taken from the range 0.05 up to 1.0 pixels.

In the following, the variation of components of the rectification matrix is discussed.

Figures 5 and 6 present the standard deviations and mean values of all matrix components obtained for an exemplary case with the input standard deviations 0.5 pixels and for the parallel displacement of the camera (as in Fig. 4) equal to -100 mm, 0 mm and 100 mm.

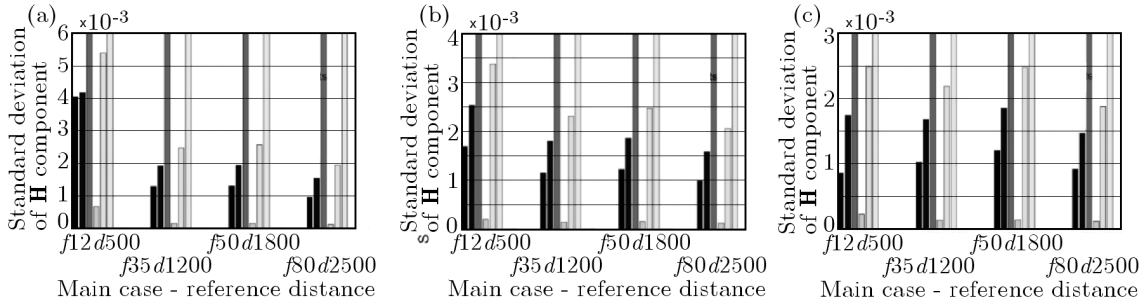


Fig. 5. Standard deviation of all components of the matrix \mathbf{H} : for parallel displacement of the camera equal to -100 mm, 0 mm and 100 mm

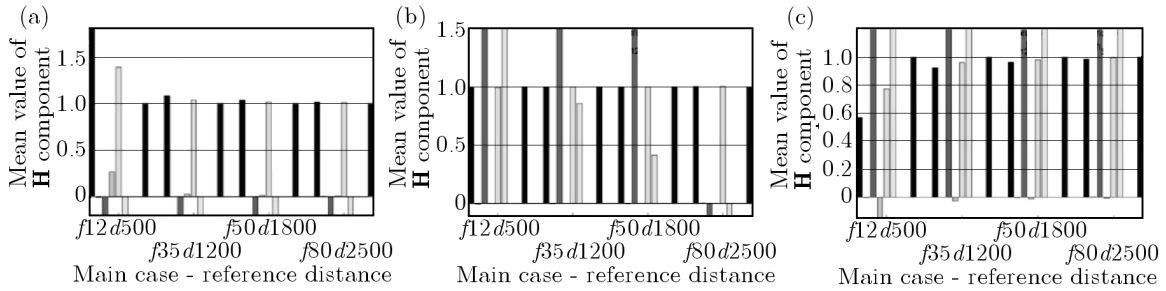


Fig. 6. Mean value of all components of the matrix \mathbf{H} : for parallel displacement of the camera equal to -100 mm, 0 mm and 100 mm

Figure 7 shows the comparison of components of the rectification matrix for an exemplary case of the reference distance 1500 mm with the focal length 50 mm and parallel displacement of the camera -100 mm. A linear relationship between the input and output resultant standard deviations irrespectively to the matrix component is observed. The linear relationship was found also for the cases of displacement equal to 0 mm and 100 mm.

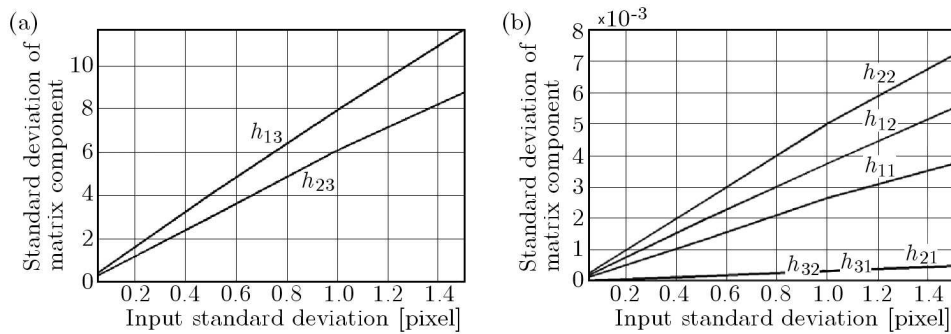


Fig. 7. Standard deviation of all components of the rectification matrix for a chosen reference case and parallel displacement -100 mm; (a) components h_{13} , h_{23} , (b) the rest of the matrix components

In Fig. 8, the variation of chosen (h_{11} and h_{23}) components of the rectification matrix for different values of the input standard deviations, the reference distance 1500 mm and the focal length 50 mm is shown. The scale on the x axis corresponds to the parallel displacement of the camera with respect to the plane of the structure. The 0 mm position is taken as the position in which the camera optical axis is perpendicular to the beam plane. Nonlinear relationships between change of the parallel displacement of the camera and resultant the standard deviation of matrix components should be noted. The above observation applies to all matrix components.

Figure 9 presents the maximum standard deviation of the static deflection of the studied beam found for all measurement points for all referential cases.

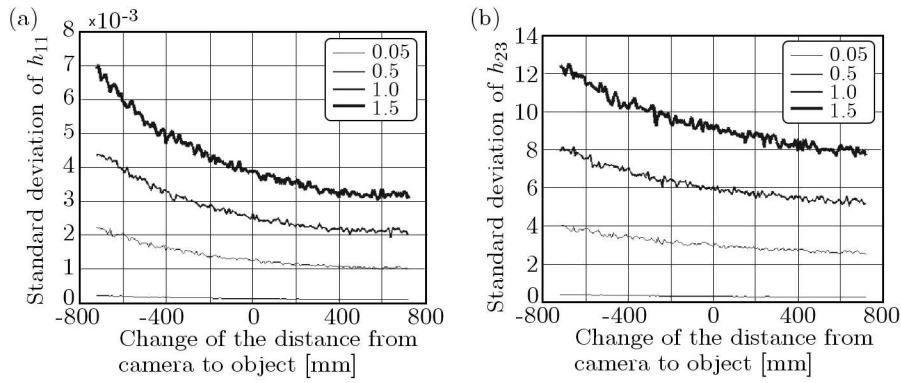


Fig. 8. (a) Standard deviation of the homography matrix element h_{11} for different standard deviations of the noise, (b) standard deviation of h_{23} for different standard deviations of the noise

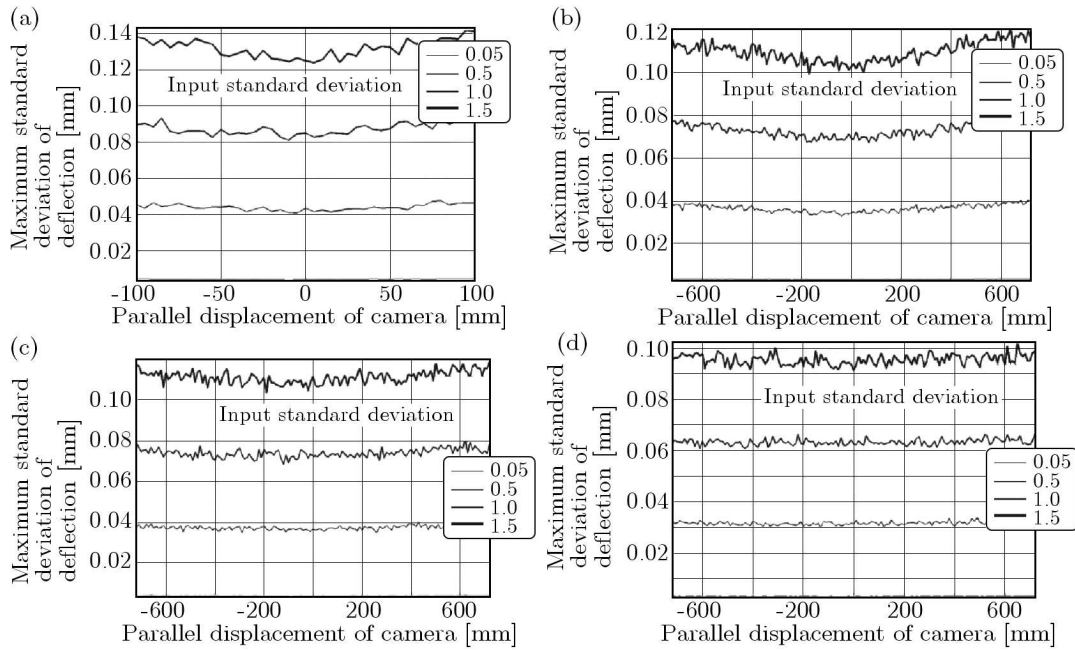


Fig. 9. Maximum standard deviation of static deflection for reference cases: (a) distance 500 mm / focal length 12 mm, (b) 1200 mm / 35 mm, (c) 1800 mm / 50 mm, (d) 2500 mm / 80 mm

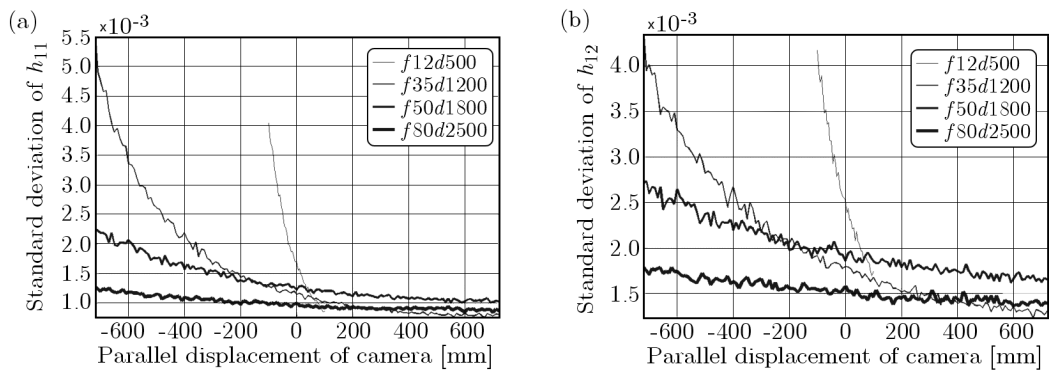


Fig. 10. Standard deviation of matrix components for all reference cases and a chosen input standard deviation 0.5 pixels

In Fig. 10, the variation of chosen components of the rectification matrix (h_{11} and h_{13}) for an exemplary case with the input standard deviations 0.5 pixels and for all cases with different focal lengths is shown.

Figure 11 shows groups of curves found for all measurement points localized along the beam and defining the standard deviation of the static deformation for all referential cases with the input standard deviations 0.5 pixels. As expected, the best accuracy can be achieved in the middle of the beam.

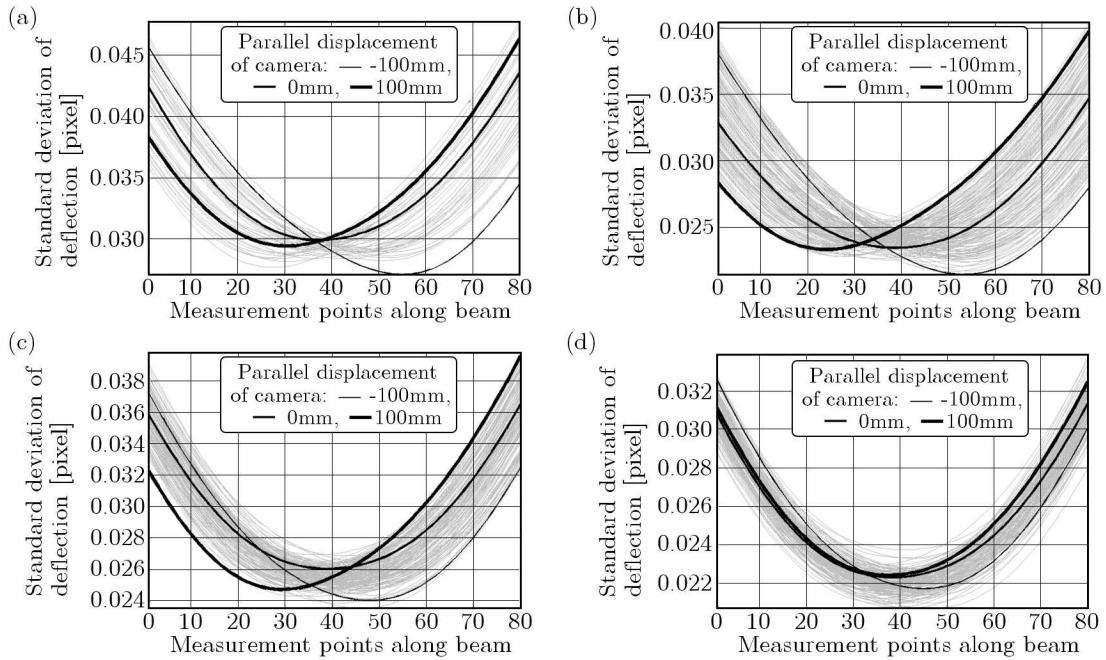


Fig. 11. Standard deviation of static deflection measured along the beam for reference cases: (a) distance 500 mm / focal length 12 mm, (b) 1200 mm / 35 mm, (c) 1800 mm / 50 mm, (d) 2500 mm / 80 mm

Figure 12 presents how the output resultant maximum standard deviation of the static deformation evolves while the input standard deviation increases for all referential cases and chosen parallel displacements of the camera. Linear relationships between the input and output standard deviations have been found irrespectively to the referential case chosen.

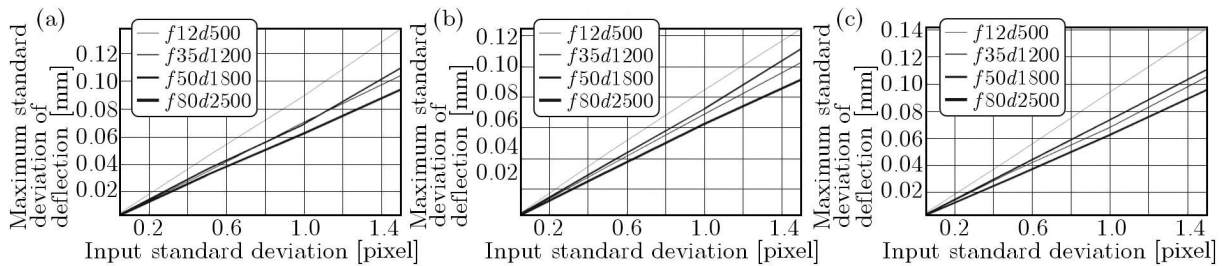


Fig. 12. Output resultant maximum standard deviation of the static deformation for parallel displacements: (a) -100 mm, (b) 0 mm, (c) 100 mm

4. Experimental tests

The lab setup (Fig. 13) consisted of an aluminum beam of length 1.8 m and cross section 50 mm × 10 mm. The beam was fixed at both ends and was loaded by a point weight acting centrally. The random intensity pattern was placed on the measured plane of the structure. The set of

rectangular markers necessary for homography matrix computation was placed coplanarly with the beam plane. Photographs of the structure were acquired by the system of two digital Canon 5D Mark II cameras with 21.1 MPix image resolution and Canon 24-70 mm $f/2.8L$ lens with focal length $f \approx 50$ mm adjusted. The optical axis of the first reference camera was perpendicular to the plane of the beam. The second camera was translated and rotated with respect to the first one, and was used for calculation of the deflection field from the images after application of the rectification.

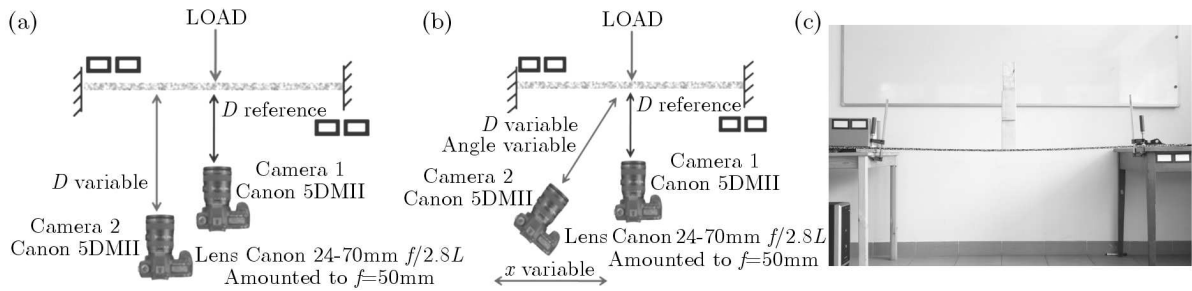


Fig. 13. Test setup: (a) first experimental test, (b) second experimental test, (c) photograph of the investigated beam

4.1. Investigation of noise characteristics

The uncertainties of the estimated horizontal and vertical positions of markers used for the homography computation were modeled by a random noise with the Gaussian distribution. In order to prove the correctness of this assumption, the uncertainty of Harris corner detector was investigated on the real images. The experimental setup consisted of a plane with 9 rectangular markers placed symmetrically with respect to each other (Fig. 14). 50 photographs of the object were acquired and all 36 corners of the rectangles were detected using the Harris corner detector. From the obtained distributions, the statistical parameters such as the mean and the standard deviation of obtained positions of vertices were calculated for the coordinates x and y of each 36 corners.

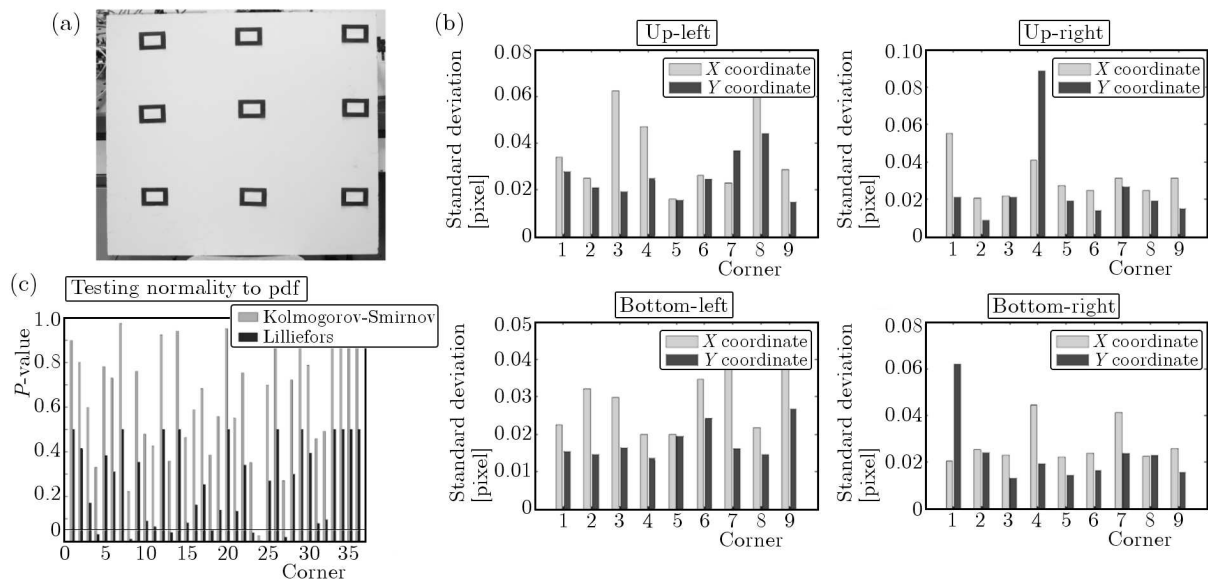


Fig. 14. (a) Investigated set-up of markers, (b) standard deviation of four corners of one rectangular marker (clockwise: upper-left, upper-right, lower-right, lower-left), (c) results of Kolmogorov-Smirnov test for all 36 vertices

The nonparametric Kolmogorov-Smirnov test for the equality of two continuous, one-dimensional probability distributions was used as an indicator of the normality of the distribution of both vertical and horizontal coordinates of each detected vertex. The test confirmed the assumed normality of the positions of features computed by means of the Harris corner detector. Figures 14b and 14c show the results of analysis.

4.2. Lab experiment results

In the first experiment, the camera was moved along an elliptical path around the structure and, at the same time, its optical axis was rotated so that it pointed at the center of the beam. The values of distances between the camera and the object as well as the corresponding angles between the optical axis and the direction perpendicular to the plane are presented in Table 2. In the second test, the camera was moved away from the object, but the orientation of its optical axis was not varied (Table 2). In both cases, the focal length of the camera was fixed and amounted to $f = 50$ mm.

Table 2. Distances and corresponding angles of the optical axis with respect to the direction perpendicular to the beam plane for two experimental cases

Lab Test 1 – distance d and corresponding angle	Lab Test 2 – distance of the camera
$d = 2800$ mm, angle = 0 deg	$d = 2800$ mm
$d = 2750$ mm, angle = 5 deg	$d = 3000$ mm
$d = 2750$ mm, angle = 10 deg	$d = 3400$ mm
$d = 2700$ mm, angle = 15 deg	$d = 3700$ mm
$d = 2600$ mm, angle = 20 deg	$d = 4000$ mm
$d = 2500$ mm, angle = 30 deg	
$d = 2400$ mm, angle = 35 deg	
$d = 2200$ mm, angle = 45 deg	

Figures 15 and 16 present standard deviations and mean values of the deflection measured along the beam for different angles of camera orientations and distances from the camera to the object (Table 2). Figure 17 presents the scatter of the standard deviation of the static deflection found for all measurement cases.

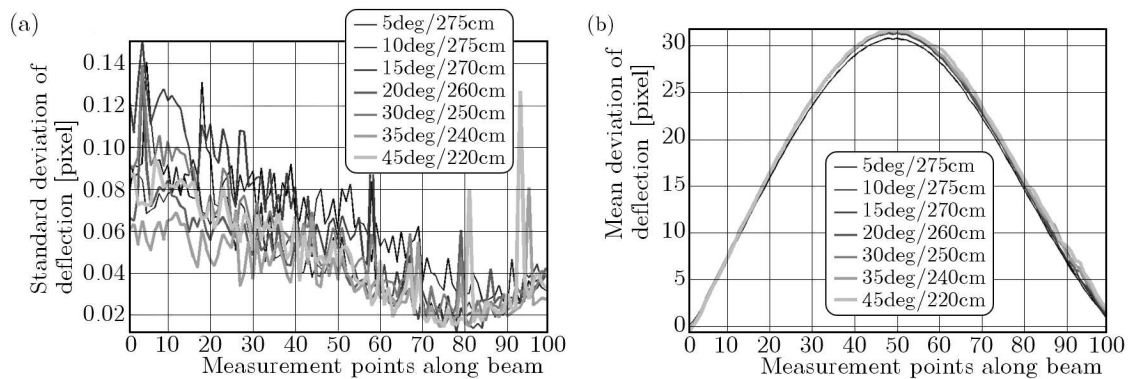


Fig. 15. Standard deviation (a) and mean values (b) of static deflection measured along the beam for different angles of camera orientation

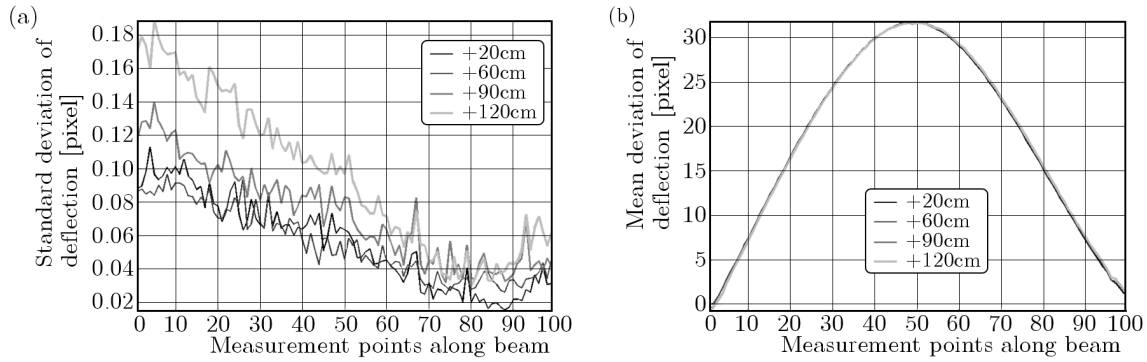


Fig. 16. Standard deviation (a) and mean values (b) of static deflection measured along the beam for different distance from the camera to the object

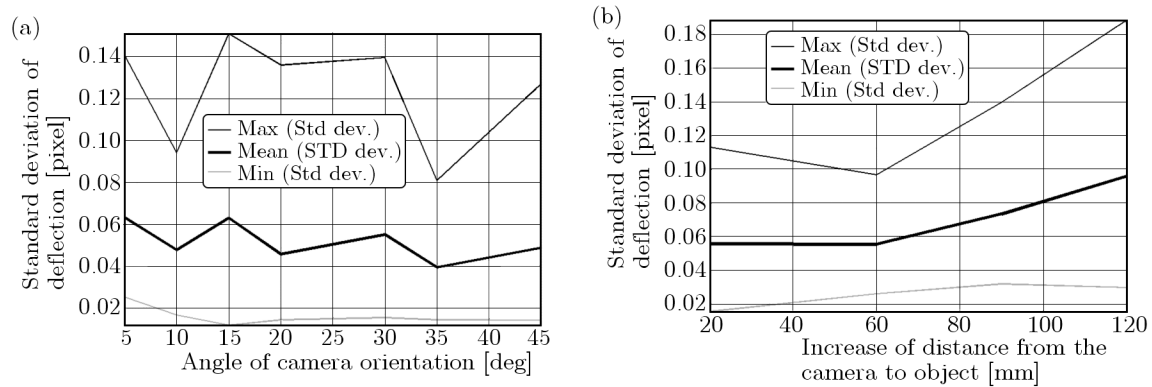


Fig. 17. Scatter of the standard deviation of static deflection: (a) for different camera orientations with respect to the structure, (b) for different distances from the camera to the object

5. Conclusions

The relationship between the standard deviation value of the input to the algorithm (corners positions) and the standard deviation of the output (homography components) has been linear. The nonlinear relationship between the change in the position of the camera with respect to the object and the standard deviation of matrix elements was evident only for the camera with the focal length less than 35 mm. Another very important observation has indicated that the standard deviation of the deflection is less than the standard deviation of corner positions for all cases of the input noise level. The largest impact of the input noise has been observed on the end points of the beam. It is reasonable, since in that region there are the smallest displacements of points, and their measurement is easily disturbed by noise in the image. The highest value of the standard deviation of the deflection has been found for the focal length $f = 12$ mm, irrespective of the chosen point of measurement. However, the effect of noise imposed on the corresponding points has been insignificant in all other cases. The standard deviation of the deflection in each measurement point has been a function of the camera parallel displacement for all considered focal lengths. For example, if the camera was moved by a distance -100 mm with respect to the central position, the standard deviation of points located on the beam left side was much larger than the right side standard deviation. However, the maximum variation of the measured deflection, captured on both ends of the beam, was constant irrespective of the camera displacement.

The experiment on the lab set-up has confirmed the results obtained from the numerical tests. In the case of the camera orbiting around the structure, the measurement of the displacement was characterized by a higher value of standard deviation for the points placed on the left side of

the beam. The calculated uncertainty was not only the result of homography computation from noisy data but came from the phenomena associated with lens design like depth of the field or radial and tangential distortions. Concerning the variable distance between the camera and the object, the standard deviation increased with the distance as expected. The highest value of the standard deviation was less than 0.18 pixels. The experiment confirmed that the mean, maximum and minimum value of the standard deviation measured along the beam length, was constant irrespective of the angle between the camera optical axis and the direction perpendicular to the beam plane. These parameters increased with the distance between the camera and the object.

The research proved that the homography transformation can be introduced to vision measurement systems for image rectification, however the application of small focal lengths is not recommended. The technique of the in-plane deflection measurement presented in this paper enables taking images of a structure from different points of view during examination. Simplification of the measurement procedure is possible because the complicated, expensive and time-consuming stage of camera positioning is not necessary.

References

1. BORNERT M., BRÉMAND F., DOUMALIN P., DUPRÉ J.C., FAZZINI M., GRÉDIAC M., HILD F., MISTOU S., MOLIMARD J., ORTEU J.-J., ROBERT L., SURREL Y., VACHER P., WATTRISSE B., 2009, Assessment of digital image correlation measurement errors: methodology and results, *Experimental Mechanics*, **49**, 3, 353-370
2. DE CHU T.C., RANSON W.F., SUTTON M.A., PETERS W.H., 1985, Application of digital-image correlation techniques to experimental mechanics, *Experimental Mechanics*, **25**, 232-244
3. DONDEERS S., VANDEPITTE D., VAN DE PEER J., DESMET W., 2005, Assessment of uncertainty on structural dynamic responses with the short transformation method, *Journal of Sound and Vibration*, **288**, 523-549
4. DUBOIS D., PRADE H., 1980, *Fuzzy Sets and Systems. Theory and Applications*, Academic Press, New York
5. GIERGIEL M., KOHUT P., 2008, Optical measurement of amplitude of vibration of machine, *Mechanics and Mechanical Engineering*, **12**, 2, 147-156
6. GIURGIUTIU V., 2008, *Structural Health Monitoring with Piezoelectric Wafer Active Sensors*, Amsterdam, Boston: Elsevier Academic Press
7. HANSS M., 2005, *Applied Fuzzy Arithmetic. An Introduction with Engineering Applications*, Springer-Verlag, Berlin
8. HARTLEY R., ZISSERMAN A., 2004, *Multiple View Geometry in Computer Vision*, Cambridge University Press
9. MA Y., SOATTO S., KOSETSKA J., SASTRY S., 2004, *An Invitation to 3D Computer Vision*, Springer-Verlag, New York
10. MOENS D., VANDEPITTE D., 2005, A survey of non-probabilistic uncertainty treatment in finite element analysis, *Computer Methods in Applied Mechanics and Engineering*, **194**, 1527-1555
11. MOENS D., VANDEPITTE D., 2006, Interval sensitivity analysis of dynamic response envelopes for uncertain mechanical structures, *Proc. of III ECCM – European Conference on Computational Mechanics*, Lisbon, Portugal
12. ORTEU J.-J., 2009, Assessment of digital image correlation measurement errors: methodology and results, *Experimental Mechanics*, **49**, 3, 353-370
13. SANTO M., LIGUORI C., PAOLILLO A., PIETROSANTO A., 2004, Standard uncertainty evaluation in image-based measurements, *Mwasurement*, **36**, 3/4, 347-358

14. SCHUELLER G.I., 1997, A state-of-the-art report on computational stochastic mechanics, *Probabilistic Engineering Mechanics*, **12**, 4, 197-321
15. UHL T., 2009, SHM of civil structures – methods, tools and applications, *EVACES'09 Proc. of the International Conference on Experimental Vibration Analysis for Civil Engineering Structures*, Wrocław, Poland, Dolnośląskie Wydawnictwo Edukacyjne, 73-92
16. UHL T., KOHUT P., HOLAK K., 2009a, Image correlation and homography mapping in optical deflection measurement, *OPTIMESS, Proc. of the 4th international conference on Optical Measurement Techniques for Structures and Systems*, Antwerp, Belgium, 191-200
17. UHL T., KOHUT.P, SZWEDO M., HOLAK K., 2009b, Static and dynamic optical measurement in SHM of civil structures, *Proceeding of the 7th International Workshop on Structural Health Monitoring*, DESTech publications, Lancaster, 1765-1773

**Analiza propagacji niepewności w opracowanym wizyjnym systemie pomiarowym
wspomagana przez testy numeryczne i eksperymentalne**

Streszczenie

W pracy przedstawiono wizyjną metodę pomiaru statycznego ugięcia konstrukcji. Przemieszczenia punktów pomiarowych wyznaczone są z wykorzystaniem znormalizowanego współczynnika korelacji wzajemnej. Zastosowanie przekształcenia homograficznego umożliwiło pomiar pola przemieszczeń na podstawie fotografii konstrukcji wykonanej z dowolnego punktu przestrzeni. W celu zwiększenia stopnia automatyzacji metody wprowadzono algorytmy wyznaczania współczynnika skali oraz dopasowania znaczników. W pracy zaprezentowano wyniki symulacji numerycznych propagacji niepewności w proponowanym algorytmie. Pokazano wyniki jakościowego porównania danych symulacyjnych i wyników eksperymentalnych.

Manuscript received October 12, 2011; accepted for print February 24, 2012